

Stacked-Layer Heterostructure Films of 2D Thiophene Nanosheets and Graphene for High-Rate All-Solid-State Pseudocapacitors with Enhanced Volumetric Capacitance

Zhong-Shuai Wu,* Yijun Zheng, Shuanghao Zheng, Sen Wang, Chenglin Sun, Khaled Parvez, Taichi Ikeda, Xinhe Bao, Klaus Müllen,* and Xinliang Feng*

With the dramatic developments of portable and wearable electronics, future energy storage devices become not only thin, light, and cheap, but also ultraflexible.^[1–6] All-solid-state supercapacitors (ASSSs) with robust mechanical flexibility and safety are considered as one competitive alternative to high power sources for full integration into the manufacturing process of electronics.^[7–10] In general, nanocarbon-based capacitive ASSSs (e.g., activated carbon,^[11] carbon nanotube,^[12] graphene^[13–15]) exhibit low volumetric capacitance,^[16] while pseudocapacitive ASSSs based on conducting polymers and metal oxides show poor rate capability and cycling stability, which greatly limit their practical applications.^[17,18] To overcome these severe drawbacks, nanocarbon-based composites with conducting polymers or metal oxides are constructed to form novel electrode

materials, realizing large volumetric capacitance, excellent rate capability, and high cyclability.^[19–22]

Recently, 2D materials, such as graphene^[23] and analogous nanosheets (e.g., metal oxides),^[24,25] are becoming a groundbreaking material platform for constructing new flexible ASSSs because of their large surface area, high mechanical flexibility, ultra-thinness, good electrical conductivity, and high theoretical capacitance (e.g., $\approx 550 \text{ F g}^{-1}$ for graphene).^[3,26–30] From this viewpoint, one promising approach for fabricating superior ASSSs is to manufacture advanced graphene-based heterostructure film electrodes assembled with 2D redox-active nanosheets in a controllable stacked order, which may lead to a significant improvement of the pseudocapacitance from conducting polymer (or transition metal oxide) nanosheets.^[19,31] Importantly, such stacked-layer heterostructure films promise high accessible surface area, excellent electrical conductivity, densely packed, and rapid electron transport in conducting nanosheets, together with fast ion diffusion in the lamellar permeable spaces. These features are desirable for achieving high volumetric capacitance and rate capability of ASSSs.^[3,25] Nevertheless, constructing heterostructure films from ultrathin pseudocapacitive polymer nanosheets and graphene for flexible ASSSs has not yet been reported.

Herein, we demonstrate the first fabrication of stacked-layer heterostructure films (denoted as TP/EG) from thiophene (TP) nanosheets and electrochemically exfoliated graphene (EG) for high-rate and flexible ASSSs (TP/EG-ASSSs) and micro-supercapacitors (TP/EG-MSCs) with superior rate capability and enhanced volumetric capacitance. The heterostructure films with a thickness of $\approx 105 \text{ nm}$ are produced by alternating deposition of electrochemically EG nanosheets (≤ 3 layers) and redox-active conducting TP nanosheets (thickness of 3.5 nm) in sequence, and exhibit large-area uniformity. Notably, the produced films were directly transferred on a polyethylene terephthalate (PET) substrate and served as binder- and additive-free electrodes for flexible supercapacitors. Remarkably, the resulting TP/EG-ASSSs exhibited a pronounced pseudocapacitance contribution with strong redox peaks, and delivered an areal capacitance of $\approx 3.9 \text{ mF cm}^{-2}$ and a volumetric capacitance of $\approx 375 \text{ F cm}^{-3}$, energy density of 13 mWh cm^{-3} and power density of 776 W cm^{-3} . Meanwhile, the TP/EG-MSCs can be operated at high rate of up to 1000 V s^{-1} , offering ultrahigh rate capability, e.g., with a landmark areal capacitance of 1.30 mF cm^{-2} and volumetric capacitance of 123 F cm^{-3} at 100 V s^{-1} , as well as unprecedented flexibility under different bending states.

Prof. Z.-S. Wu, S. H. Zheng, S. Wang, Prof. C. L. Sun,

Prof. X. H. Bao

Dalian National Laboratory for Clean Energy

Dalian Institute of Chemical Physics

Chinese Academy of Sciences

457 Zhongshan Road, Dalian 116023, China

E-mail: wuzs@dicp.ac.cn

Dr. Y. J. Zheng

Leibniz Institute for New Materials

Campus D2 2, 66123 Saarbrücken, Germany

S. H. Zheng, Prof. X. H. Bao

State Key Laboratory of Catalysis

iChEM

Dalian Institute of Chemical Physics

Chinese Academy of Sciences

457 Zhongshan Road, Dalian 116023, China

S. H. Zheng, S. Wang

University of Chinese Academy of Sciences

19 A Yuquan Rd, Shijingshan District, Beijing 100039, China

Dr. K. Parvez, Prof. K. Müllen

Max-Planck-Institut für Polymerforschung

Ackermannweg 10, 55128 Mainz, Germany

E-mail: muellen@mpip-mainz.mpg.de

Dr. T. Ikeda

Research Center for Functional Materials

National Institute for Materials Science (NIMS)

Namiki 1-1, Tsukuba, Ibaraki 305-0044, Japan

Prof. X. L. Feng

Center for Advancing Electronics Dresden (cfaed)

and Department of Chemistry and Food Chemistry

Technische Universität Dresden

01062 Dresden, Germany

E-mail: xinliang.feng@tu-dresden.de



DOI: 10.1002/adma.201602960

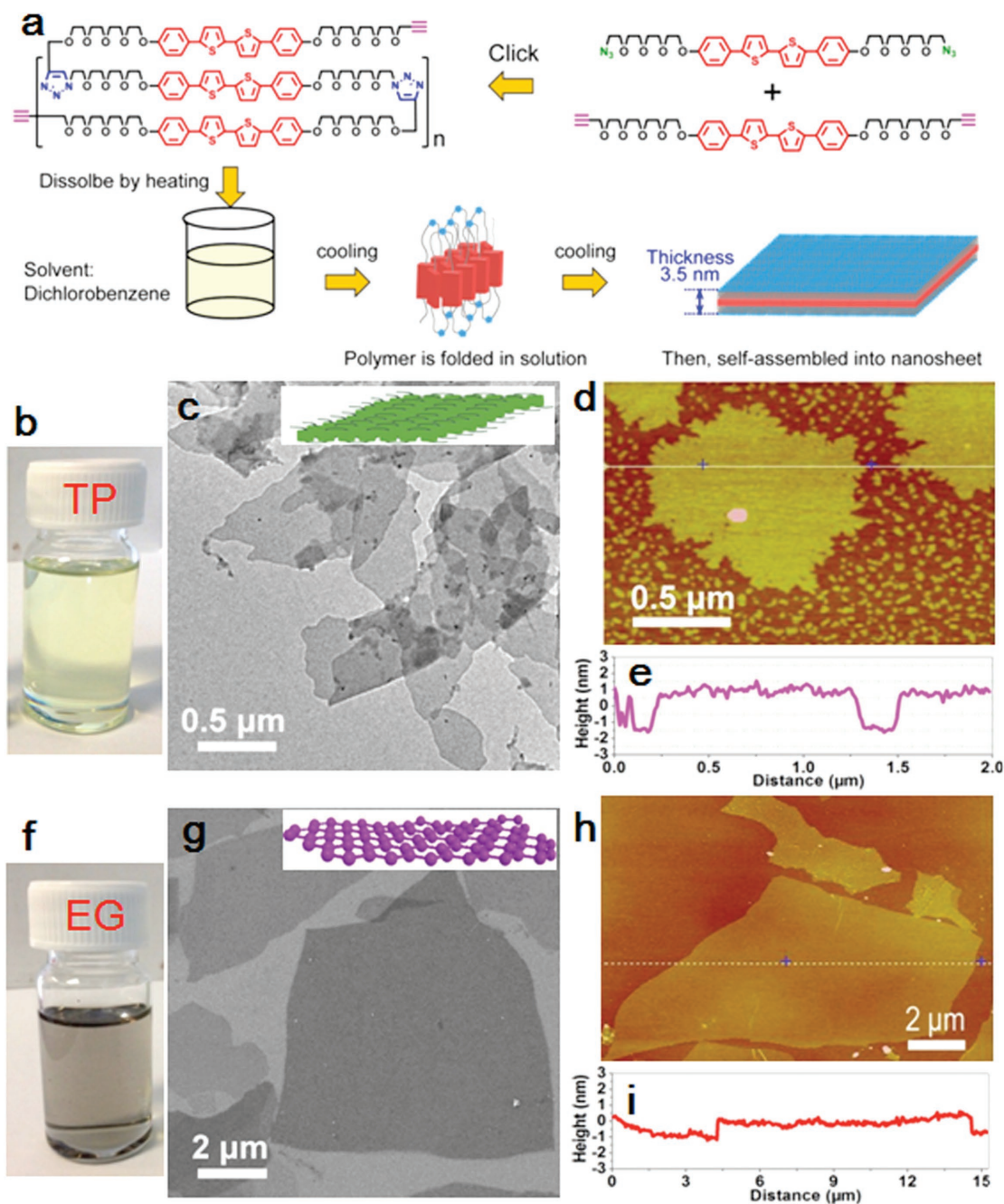


Figure 1. Structural and morphological characterization of the TP and EG nanosheets. a) Fabrication of TP nanosheets by self-assembly of the polymer consisting of the Ph₂TPh monomers linked by 1,2,3-triazole units in DCB. b) Optical image of the stable TP solution, 1×10^{-4} M of monomer unit concentration in DCB. c) TEM image of TP nanosheets (Inset is the schematic description of TP). d) AFM image and e) height profile of TP nanosheets, thickness of ≈ 3.5 nm. f) Optical image of the stable EG solution, 0.1 mg mL^{-1} in DMF. g) SEM image of EG nanosheets (Inset is the schematic of EG nanosheet). h) AFM image and i) height profile of EG nanosheets, thickness of ≈ 1.0 nm.

To construct the stacked-layer heterostructure film, we selected two types of different solution-processable nanosheets: one is the redox TP nanosheets (Figure 1a–e), and the other one is the capacitive EG nanosheets (Figure 1f–i). The 2D redox TP nanosheets were fabricated by hierarchical self-assembly of the polymer consisting of the tetra(ethylene glycol)-disubstituted phenyl-capped bithiophene (Ph₂TPh) monomers linked

by 1,2,3-triazole units in 1,2-dichlorobenzene (DCB) solvent through artificial polymer folding, in which the TP units are stacked with each other and the folded copolymer further self-assembled into a 2D sheet structure (Figure 1a–e, Figures S1 and S2, See Experimental Section in the Supporting Information).^[32–34] Since the copolymer has the folded conformation, the single-layer TP nanosheet has a thickness of about 3.5 nm,

as confirmed by atomic force microscopy (AFM, Figure 1d,e), and a lamellar structure, as revealed by wide-angle X-ray scattering measurements.^[32] Transmission electron microscopy (TEM, Figure 1c, Figure S1, Supporting Information), scanning electron microscopy (SEM, Figure S2, Supporting Information) and AFM (Figure 1d,e) images show the lateral size ranging from submicrometer to several micrometers. It should be mentioned that TP is one of the advanced active materials for high-capacitance pseudocapacitors,^[35–38] particularly with the fabricated 2D TP nanosheets holding great promise for electrochemical energy storage. On the other hand, electrochemically EG nanosheets with high conductivity and good solution processability were chosen to process uniform thin films for flexible supercapacitors. To this end, a straightforward and fast electrochemical protocol was applied for direct exfoliation of graphite into high-quality EG sheets (Figure 1f–i, See Experimental Section in the Supporting Information).^[39] The fabricated EG nanosheets have a high yield (>80% of ≤ 3 layers), large lateral size (10 μm), high electrical conductivity, and excellent solution processability (e.g., 1 mg mL^{-1} in *N,N'*-dimethylformamide

(DMF)), which are favorable for manufacturing large-area and highly conductive heterostructure films.^[40]

Subsequently, the TP/EG heterostructure films were fabricated by alternating deposition of the TP nanosheets in DCB and EG nanosheets in DMF in a controlled sequence, and subsequently dry-transferred on Au-coated PET substrates (Inset in Figure 2a). Using this approach, large scale, continuous, uniform heterostructure films were readily produced. For instance, a film with a stacked-layer EG/TP/EG/TP/EG structure (Figure S3, Supporting Information), and a thickness of around 105 nm (Figure 2b,c), was obtained by alternating depositing each dispersion of EG (5 mL, 0.1 mg mL^{-1} , three times) and TP nanosheets (5 mL, 1×10^{-4} M of monomer unit concentration, two times) (lower inset in Figure 2a). Interestingly, the large-area continuous EG layers, as shown in Figure 2d, could provide enough spatial confinement making the adjacent redox TP layers spatially separate in between the adjacent capacitive EG layers. Moreover, the obtained TP/EG films presented high electrical conductivity of 40 S cm^{-1} , measured by a standard four-point probe system. Further, the

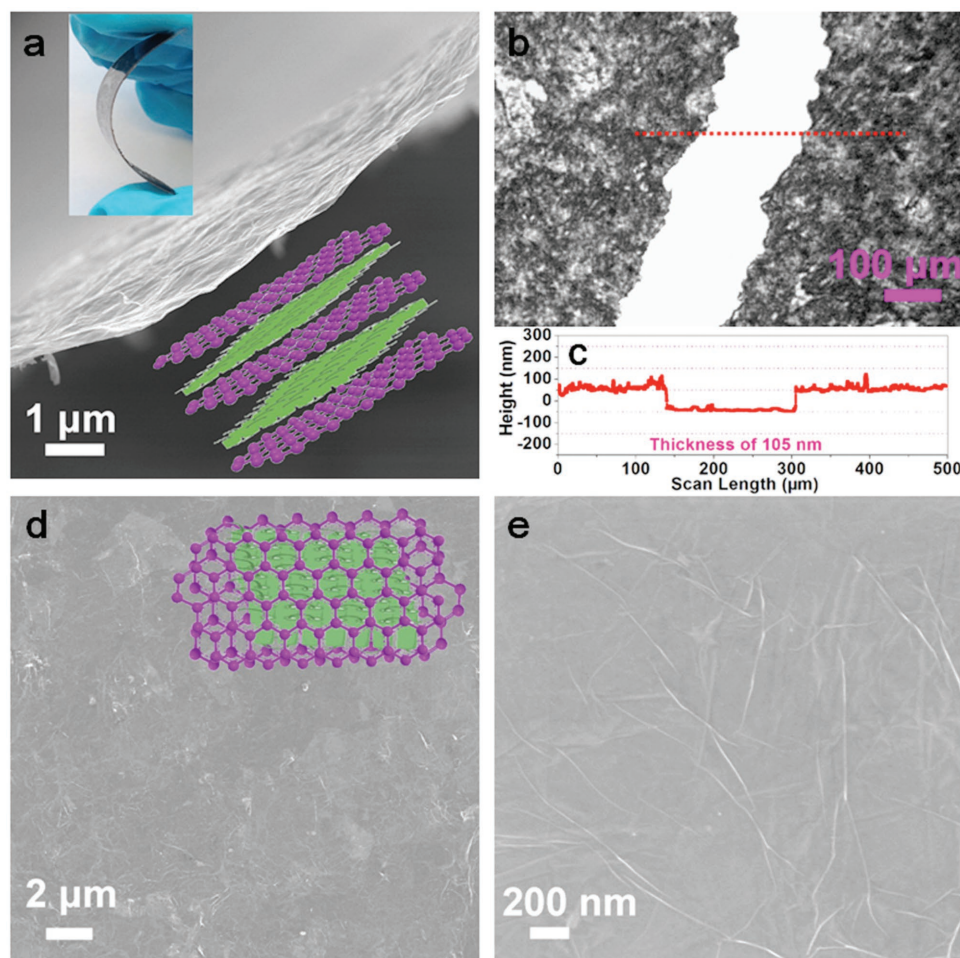


Figure 2. Characterization of the TP/EG heterostructure film. a) SEM image of the freestanding TP/EG heterostructure film (Top-left inset is the as-prepared film on PET substrate, and the bottom-right inset is the scheme of the heterostructure film). b) The surface morphology and c) the corresponding thickness of the TP/EG heterostructure films measured by the step profiler. d) The top-view SEM image of the TP/EG heterostructure films (Inset is the scheme of the heterostructure film). e) The top-view SEM image of the TP/EG heterostructure films with high magnification, showing the presence of the wrinkles from graphene.

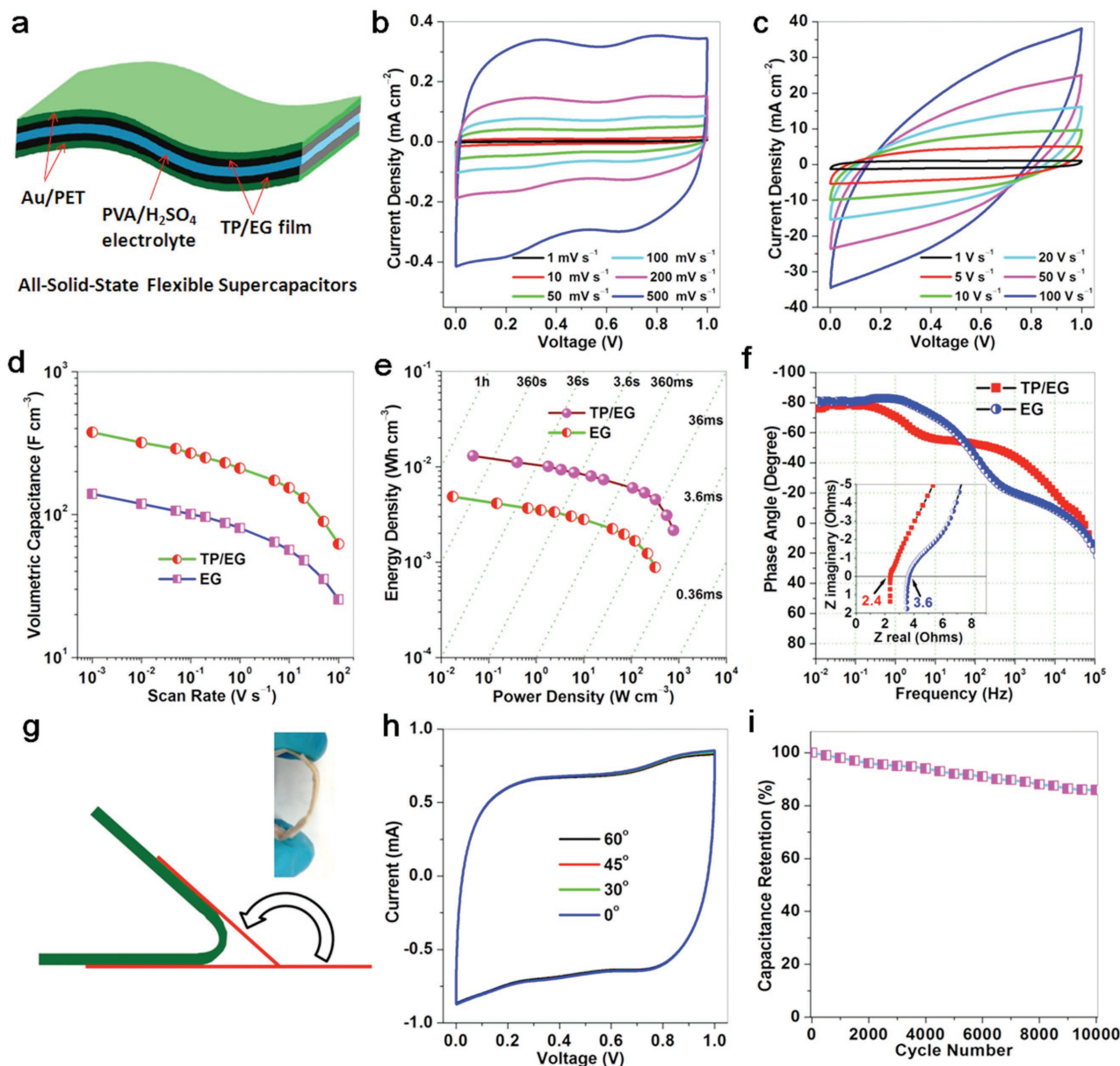


Figure 3. Electrochemical characterization of the TP/EG-ASSSs. a) The scheme of flexible TP/EG-ASSSs. b,c) CV curves of TP/EG-ASSSs obtained at different scan rates (b) from 1 to 500 mV s^{-1} , and (c) from 1 to 100 V s^{-1} . d) Volumetric capacitance of the TP/EG-ASSSs and EG-ASSSs. e) Ragone plot of the TP/EG-ASSSs and EG-ASSSs. f) Impedance phase angle as a function of frequency for TP/EG-ASSSs and EG-ASSSs. Inset is the high-frequency Nyquist plot of TP/EG-ASSSs and EG-ASSSs. g) The bending scheme and h) the CVs of TP/EG-ASSSs tested under different bending degrees. i) The cycling stability of the TP/EG-ASSSs measured at a scan rate of 100 mV s^{-1} .

as-fabricated heterostructure films with rich nanoporous structure (Figure S4, Supporting Information) as electrodes for supercapacitors are free of polymer binder and carbon additive, and exhibited a pronounced redox response (Figure S5, Supporting Information) and good stability in acidic gel electrolyte of polyvinyl alcohol (PVA)/ H_2SO_4 (Figure S6, Supporting Information). Given the above advantages, the flexible TP/EG-ASSSs were first assembled by two as-fabricated heterostructure films on Au-coated PET substrates as the working electrodes, in which the gel of PVA/ H_2SO_4 acting as both electrolyte and thin separator was sandwiched in between them.^[41] Finally, the

flexible pseudocapacitor was obtained with an electrode-separator-electrolyte integrated structure (Figure 3a).

The electrochemical behavior of the resultant TP/EG-ASSSs was evaluated by means of cyclical voltammograms (CV) at different scan rates from 1 mV s^{-1} to 100 V s^{-1} (Figure 3b,c). For comparison, ASSSs based on EG films (a thickness of ≈ 100 nm, denoted as EG-ASSSs) were assembled under the same procedure, without involvement of the TP component. Apparently, the TP/EG-ASSSs exhibited pronounced redox peaks particularly at low scan rate from 1 to 500 mV s^{-1} , corresponding to the pseudocapacitive reaction of TP layers

(Figure 3b, Figure S5, Supporting Information). In sharp contrast, the CVs of EG-ASSSs presented a typical box-like shape, indicating electric double layer capacitive behavior (Figure S7, Supporting Information). Notably, the TP/EG-ASSSs showed higher areal capacitance of 3.9 mF cm^{-2} , in comparison with EG-ASSSs, 1.5 mF cm^{-2} at 1 mV s^{-1} . Further, the TP/EG-ASSSs (2.4 mF cm^{-2} at 500 mV s^{-1}) presented better rate capability than EG-ASSSs (1.0 mF cm^{-2} for at 500 mV s^{-1} , Figure S8, Supporting Information). The higher areal capacitance for TP/EG-ASSSs verified the substantial involvement of pseudocapacitive charge storage. Accordingly, the TP/EG-ASSSs delivered an ultrahigh volumetric capacitance of $\approx 375 \text{ F cm}^{-3}$, much higher than the ASSSs fabricated based on EG film (139 F cm^{-3}), activated graphene ($60\text{--}100 \text{ F cm}^{-3}$),^[42] laser scribed graphene films ($9.7\text{--}10.6 \text{ F cm}^{-3}$),^[27] and liquid-mediated graphene films (261.3 F cm^{-3}),^[3] and most conducting polymer-based films (Table S1, Supporting Information). Further, the TP/EG-ASSSs exhibited a significant volumetric capacitance of 62 F cm^{-3} at 100 V s^{-1} (Figure 3c,d). These results further demonstrated the essential merits of the unique heterostructure films for energy storage.

The Ragone plot related to energy and power densities calculated by integrating the CV curves at different rates against the volume of two electrodes is shown in Figure 3e. Remarkably, an ultrahigh energy density of 13 mWh cm^{-3} was attained for TP/EG-ASSSs. By contrast, EG-ASSSs showed only 4.9 mWh cm^{-3} . Power densities of 776 and 317 W cm^{-3} were obtained for TP/EG-ASSSs and EG-ASSSs, respectively. As revealed by the time constants (obtained by dividing the energy density by the power density), the TP/EG film was capable of rapid storing energy, in particular, 4.5 mWh cm^{-3} for TP/EG-ASSSs could be completely recharged within an extremely short time of 50 ms , much shorter than the recharge time of $>16 \text{ min}$ for storing the same energy density for EG-ASSSs.

Electrochemical impedance spectra of the TP/EG-ASSSs and EG-ASSSs measured in a frequency range from 0.01 Hz to 100 kHz are compared in Figure 3f. Obviously, the TP/EG-ASSSs in a high frequency Nyquist plot showed an equivalent series resistance (ESR) of 2.4Ω , much smaller than that of 3.6Ω for EG-ASSSs (Inset in Figure 3f). Further, no semicircle was observed for TP/EG-ASSSs in the high-frequency region, suggestive of ultrasmall charge transfer resistance. The plot of the phase angle against the frequency reveals the characteristic frequency f_0 at the phase angle of -45° was 835 Hz for TP/EG-ASSSs, much higher than that for EG-ASSSs (98 Hz). Accordingly, the time constant τ_0 ($\tau_0 = 1/f_0$) that represents the minimum time to discharge $\geq 50\%$ of all the energy from the device was only 1.2 ms for TP/EG-ASSSs, whereas 10.2 ms was required for EG-ASSSs. The characteristics of low ESR, ultrasmall charge transfer resistance, and short time constant validated the excellent charge and discharge capability of the TP/EG-ASSSs.

To further evaluate the potential for flexible energy storage, the TP/EG-ASSSs were implemented under different bending conditions and the electrochemical performance was analyzed, as demonstrated in Figure 3g,h. It is appeared from the CVs that the bending had almost no effect on the capacitive performance. The cycling stability of TP/EG-ASSSs was measured at a scan rate of 100 mV s^{-1} for 10000 cycles (Figure 3i, Figure S9,

Supporting Information), and the capacitance showed slight degradation after long-term cycles, maintaining $\approx 86\%$ of initial capacitance, which is superior to the pure TP films for ASSSs (Figure S10, Supporting Information).

To meet the requirements for lightweight, flexible, and miniaturized electronic devices,^[8] we further demonstrate the concept of the planar MSCs (TP/EG-MSCs) using the interdigital electrodes of TP/EG heterostructure film and thus covered by a PVA/H₂SO₄ gel electrolyte (See details in the Supporting Information). Note that the widths of the well-defined interdigitated fingers and interspace are of ≈ 210 and $\approx 70 \mu\text{m}$, respectively (Figure S11, Supporting Information). Figure 4a,b illustrates the planar device geometry and fast charge-discharge mechanism of the resultant TP/EG-MSCs, respectively. The CV curves measured at low scan rates, e.g., 100 mV s^{-1} , exhibited an impressive pseudocapacitive behavior due to the presence of TP nanosheets. Notably, the fabricated microdevice could perform well in a wide range of scan rates up to 1000 V s^{-1} , ten times higher than that of the sandwiched TP/EG-ASSSs (Figure 3b,c). This is essentially attributed to the synergetic effect of planar device geometry with ultrashort ion diffusion pathway and the strong coupling of both 2D TP nanosheet and graphene in heterostructure film, allowing for ultrafast transport of the electrolyte ions along the planar surface of nanosheets (Figure 4b). The areal capacitance and volumetric capacitance of TP/EG-MSCs as a function of scan rates are given in Figure 4d. Remarkably, the TP/EG-MSCs delivered an areal capacitance of 3.42 mF cm^{-2} and volumetric capacitance of 326 F cm^{-3} at 10 mV s^{-1} , both of which are superior to those of the sandwiched TP/EG-ASSSs (3.35 mF cm^{-2} and 319 F cm^{-3}). More importantly, the resultant MSCs offered a higher capacitance operated at a high rate. For instance, 1.30 mF cm^{-2} and 123 F cm^{-3} were obtained at 100 V s^{-1} . On the contrary, the specific capacitance of the sandwiched TP/EG-ASSSs declined quickly, exhibiting much lower capacitances at the same rate (Figure 3d). In addition, the TP/EG-MSCs exhibited good electrochemical stability under a flat and bending state, and 97% of the capacitance in a flat state was kept even at a bending degree of 180° (Figure 4e).

The outstanding electrochemical performance of the TP/EG-based compact supercapacitors is attributed to the unique stacked-layer heterostructure film with an integrated synergetic effect of ultrathin pseudocapacitive TP nanosheets and capacitive EG nanosheets: First, the heterostructure films feature high electron conducting pathway of EG layer, 2D parallel ion channels between the EG and TP layers. Note that these key advantages can maximize the utilization of the high surface area of ultrathin 2D nanosheets for accelerating fast surface redox reaction and ion adsorption. As a result, they can remarkably bring in additional pseudocapacitance and electrical double layer capacitance.^[19] Second, the EG nanosheets sandwiched between redox TP layers not only serve as the electrical double active layer for delivering capacitance,^[43] but also as the electrically conductive layer for rapid electron transport, leading to high rate capability. Third, the ultra-thinness and mechanically flexibility of the 2D nanosheets in the established heterostructure film could efficiently form a densely packed film, which benefits for the enhancement of the volumetric capacitance and the flexibility of thin film supercapacitors.^[40,44]

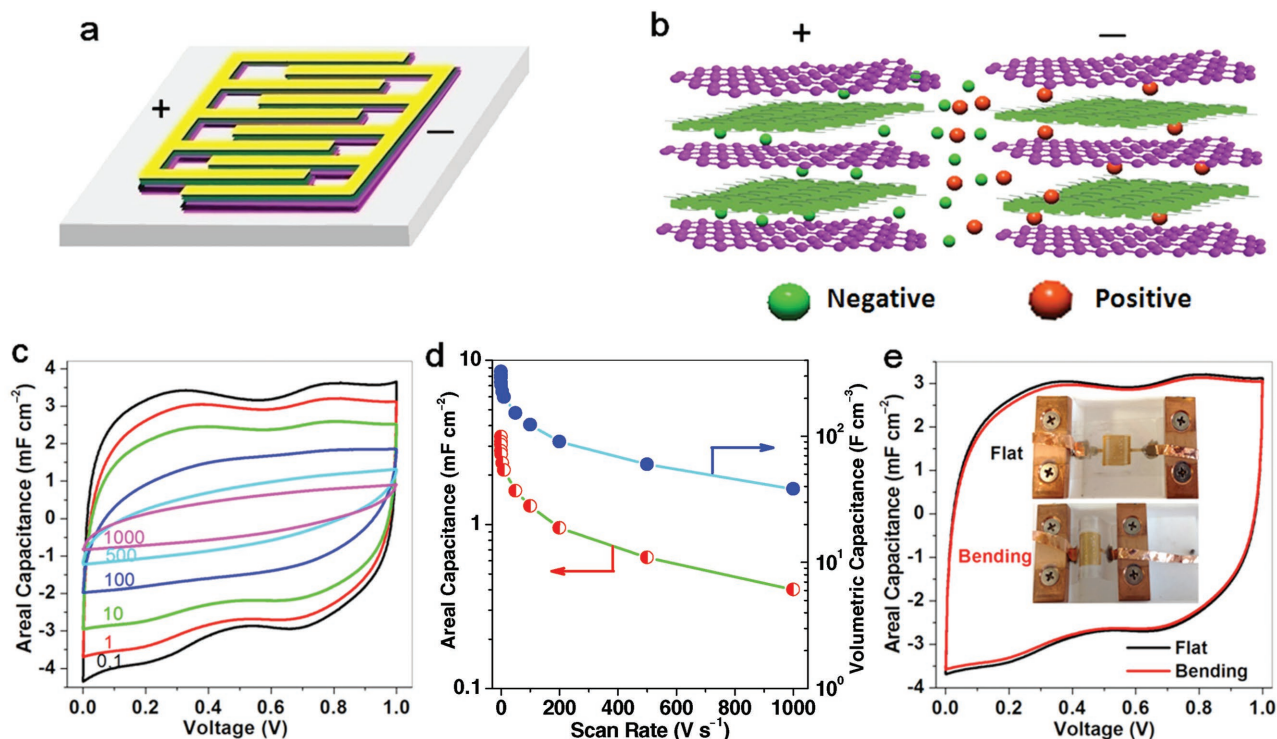


Figure 4. Electrochemical characterization of the TP/EG-MSCs. a,b) Scheme of (a) the planar TP/EG-MSCs in top view and (b) side view of charging state, respectively. c) CV curves of TP/EG-MSCs obtained at different scan rates from 0.1 to 1000 V s⁻¹. d) The areal capacitance and volumetric capacitance of TP/EG-MSCs as a function of scan rate. e) CV curves of TP/EG-MSCs obtained at 1 V s⁻¹ under flat and bending state. Inset: the photographs of the TP/EG-MSCs under flat and bending states.

In summary, we demonstrate the fabrication of high-performance all-solid-state pseudocapacitors and MSCs based on the 2D heterostructure film of ultrathin TP and EG nanosheets, in which the assembled TP/EG-ASSSs exhibited impressive volumetric capacitance, high energy density, and power density, and TP/EG-MSCs showed superior rate capability working well up to 1000 V s⁻¹ and remarkable flexibility under different bending states. This new stacked-layer heterostructures films, with an integrated synergistic effect of ultrathin pseudocapacitive TP nanosheets and capacitive EG nanosheets, guarantee fast ion diffusion and electron transport throughout the binder-free compact film electrode. We believe that this strategy of assembling stacked-layer heterostructure films will open up novel possibility for realizing 2D graphene and analogous redox nanosheets for new-concept thin-film energy storage devices.

Supporting Information

Supporting Information is available from the Wiley Online Library or from the author.

Acknowledgements

This work was financially supported by the Thousand Youth Talents Plan of China, Ministry of Science and Technology of China (Grants Nos. 2016YBF0100100 and 2016YFA0200200), National Natural Science Foundation of China (Grant No. 51572259), Natural Science

Foundation of Liaoning Province (Grant No. 201602737), DICP (Grant No. Y5610121T3), ERC Grant on 2DMATER and EC under Graphene Flagship (Grant No. CNECT-ICT-604391).

Received: June 4, 2016
Revised: August 28, 2016
Published online: November 15, 2016

- [1] C. Liu, F. Li, L. P. Ma, H. M. Cheng, *Adv. Mater.* **2010**, *22*, E28.
- [2] Y. N. Meng, Y. Zhao, C. G. Hu, H. H. Cheng, Y. Hu, Z. P. Zhang, G. Q. Shi, L. T. Qu, *Adv. Mater.* **2013**, *25*, 2326.
- [3] X. W. Yang, C. Cheng, Y. F. Wang, L. Qiu, D. Li, *Science* **2013**, *341*, 534.
- [4] D. Yu, K. Goh, H. Wang, L. Wei, W. Jiang, Q. Zhang, L. Dai, Y. Chen, *Nat. Nanotechnol.* **2014**, *9*, 555.
- [5] G. Sun, J. Liu, X. Zhang, X. Wang, H. Li, Y. Yu, W. Huang, H. Zhang, P. Chen, *Angew. Chem. Int. Ed.* **2014**, *53*, 12576.
- [6] L. Wen, F. Li, H.-M. Cheng, *Adv. Mater.* **2016**, *28*, 4306.
- [7] X. Wang, X. Lu, B. Liu, D. Chen, Y. Tong, G. Shen, *Adv. Mater.* **2014**, *26*, 4763.
- [8] Z.-S. Wu, Z. Liu, K. Parvez, X. Feng, K. Müllen, *Adv. Mater.* **2015**, *27*, 3669.
- [9] Z. Liu, Z.-S. Wu, S. Yang, R. Dong, X. Feng, K. Müllen, *Adv. Mater.* **2016**, *28*, 2217.
- [10] Z. Niu, W. Zhou, X. Chen, J. Chen, S. Xie, *Adv. Mater.* **2015**, *27*, 6002.
- [11] S. Zhai, W. Jiang, L. Wei, H. E. Karahan, Y. Yuan, A. K. Ng, Y. Chen, *Mater. Horiz.* **2015**, *2*, 598.
- [12] Y. J. Kang, S. J. Chun, S. S. Lee, B. Y. Kim, J. H. Kim, H. Chung, S. Y. Lee, W. Kim, *ACS Nano* **2012**, *6*, 6400.

- [13] Z. Weng, Y. Su, D. W. Wang, F. Li, J. H. Du, H. M. Cheng, *Adv. Energy Mater.* **2011**, *1*, 917.
- [14] K. X. Sheng, Y. Q. Sun, C. Li, W. J. Yuan, G. Q. Shi, *Sci. Rep.* **2012**, *2*, 247.
- [15] Z.-S. Wu, K. Parvez, X. L. Feng, K. Müllen, *Nat. Commun.* **2013**, *4*, 2487.
- [16] G. Wang, H. Wang, X. Lu, Y. Ling, M. Yu, T. Zhai, Y. Tong, Y. Li, *Adv. Mater.* **2014**, *26*, 2676.
- [17] X. F. Wang, B. Liu, Q. F. Wang, W. F. Song, X. J. Hou, D. Chen, Y. B. Cheng, G. Z. Shen, *Adv. Mater.* **2013**, *25*, 1479.
- [18] Y. Zhai, Y. Dou, D. Zhao, P. F. Fulvio, R. T. Mayes, S. Dai, *Adv. Mater.* **2011**, *23*, 4828.
- [19] Z.-S. Wu, K. Parvez, S. Li, S. Yang, Z. Liu, S. Liu, X. Feng, K. Müllen, *Adv. Mater.* **2015**, *27*, 4054.
- [20] X. Cao, B. Zheng, W. Shi, J. Yang, Z. Fan, Z. Luo, X. Rui, B. Chen, Q. Yan, H. Zhang, *Adv. Mater.* **2015**, *27*, 4695.
- [21] J. Chen, K. X. Sheng, P. H. Luo, C. Li, G. Q. Shi, *Adv. Mater.* **2012**, *24*, 4569.
- [22] G. Sun, X. Zhang, R. Lin, J. Yang, H. Zhang, P. Chen, *Angew. Chem.-Int. Ed.* **2015**, *54*, 4651.
- [23] Z.-S. Wu, X. Feng, H.-M. Cheng, *Natl. Sci. Rev.* **2014**, *1*, 277.
- [24] H. Zhang, *ACS Nano* **2015**, *9*, 9451.
- [25] M. R. Lukatskaya, O. Mashtalir, C. E. Ren, Y. Dall'Agnese, P. Rozier, P. L. Taberna, M. Naguib, P. Simon, M. W. Barsoum, Y. Gogotsi, *Science* **2013**, *341*, 1502.
- [26] C. Z. Wu, X. L. Lu, L. L. Peng, K. Xu, X. Peng, J. L. Huang, G. H. Yu, Y. Xie, *Nat. Commun.* **2013**, *4*, 2431.
- [27] M. F. El-Kady, V. Strong, S. Dubin, R. B. Kaner, *Science* **2012**, *335*, 1326.
- [28] Z. Bo, W. G. Zhu, W. Ma, Z. H. Wen, X. R. Shuai, J. H. Chen, J. H. Yan, Z. H. Wang, K. F. Cen, X. L. Feng, *Adv. Mater.* **2013**, *25*, 5799.
- [29] X. W. Yang, J. W. Zhu, L. Qiu, D. Li, *Adv. Mater.* **2011**, *23*, 2833.
- [30] X. Cao, B. Zheng, W. Shi, J. Yang, Z. Fan, Z. Luo, X. Rui, B. Chen, Q. Yan, H. Zhang, *Adv. Mater.* **2015**, *27*, 4695.
- [31] D. Deng, K. S. Novoselov, Q. Fu, N. Zheng, Z. Tian, X. Bao, *Nat. Nanotechnol.* **2016**, *11*, 218.
- [32] Y. Zheng, H. Zhou, D. Liu, G. Floudas, M. Wagner, K. Koyinov, M. Mezger, H.-J. Butt, T. Ikeda, *Angew. Chem. Int. Ed.* **2013**, *52*, 4845.
- [33] T. Ikeda, *Langmuir* **2015**, *31*, 667.
- [34] T. Ikeda, H. Tamura, T. Sakurai, S. Seki, *Nanoscale* **2016**, *8*, 14673.
- [35] A. Laforgue, P. Simon, C. Sarrazin, J. F. Fauvarque, *J. Power Sources* **1999**, *80*, 142.
- [36] S. R. P. Gnanakan, M. Rajasekhar, A. Subramania, *Int. J. Electrochem. Sci.* **2009**, *4*, 1289.
- [37] S. R. P. Gnanakan, N. Muruganatham, A. Subramania, *Polym. Advan. Technol.* **2011**, *22*, 788.
- [38] D. Aradilla, D. Azambuja, F. Estrany, M. T. Casas, C. A. Ferreira, C. Aleman, *J. Mater. Chem.* **2012**, *22*, 13110.
- [39] K. Parvez, R. J. Li, S. R. Puniredd, Y. Hernandez, F. Hinkel, S. H. Wang, X. L. Feng, K. Müllen, *ACS Nano* **2013**, *7*, 3598.
- [40] Z.-S. Wu, S. Yang, L. Zhang, J. B. Wagner, X. Feng, K. Müllen, *Energy Storage Mater.* **2015**, *1*, 119.
- [41] Z.-S. Wu, A. Winter, L. Chen, Y. Sun, A. Turchanin, X. Feng, K. Müllen, *Adv. Mater.* **2012**, *24*, 5130.
- [42] Y. W. Zhu, S. Murali, M. D. Stoller, K. J. Ganesh, W. W. Cai, P. J. Ferreira, A. Pirkle, R. M. Wallace, K. A. Cychoz, M. Thommes, D. Su, E. A. Stach, R. S. Ruoff, *Science* **2011**, *332*, 1537.
- [43] Z.-S. Wu, K. Parvez, A. Winter, H. Vieker, X. Liu, S. Han, A. Turchanin, X. Feng, K. Müllen, *Adv. Mater.* **2014**, *26*, 4552.
- [44] M. Ghidui, M. R. Lukatskaya, M. Q. Zhao, Y. Gogotsi, M. W. Barsoum, *Nature* **2014**, *516*, 78.